Effect of an Internal Rotational Nonlinear Attachment on the Vortex-Induced Vibration of a Rigid Circular Cylinder in a Subcritical Incompressible Flow

Ravi Kumar R. Tumkur*, Arne J. Pearlstein**, Arif Masud***, Oleg V. Gendelman****, Lawrence A. Bergman*, Alexander F. Vakakis**
*Department of Aerospace Engineering
**Department of Mechanical Science and Engineering
***Department of Civil and Environmental Engineering
University of Illinois at Urbana-Champaign, Urbana, IL 61801, USA
****Faculty of Mechanical Engineering, Technion-Israel Institute of Technology, Haifa 3200, Israel

Summary. "Vortex-induced vibration" (VIV) of a sprung cylinder is a familiar fluid-structure interaction phenomenon occurring over a wide range of flow Reynolds number (Re). From a dynamical systems perspective, at critical Reynolds number (Re_c), the fixed point of the wake oscillator loses its stability resulting in limit-cycle oscillation, which is a well known supercritical Hopf bifurcation. In this paper, we discuss the relation between the critical Reynolds number (Re_c) for the Hopf bifurcation and the stiffness of the cylinder for a sprung rigid circular cylinder. In addition, we introduce a rotational "nonlinear energy sink" (NES) into the system and study its effect on Re_c in subcritical flow regime.

Formulation of coupled system with rotational NES

The essentially nonlinear device, termed the rotational NES, as discussed in [2], consists of a small mass and a viscous damper. The NES mass is constrained to rotate at a fixed radius about the oscillating center of the cylinder, with the cylinder motion constrained to be perpendicular to the mean flow. A schematic of the rotating NES attached to the cylinder is shown in Fig. 1. The damping of the NES necessary for dissipation is assumed to be a linear viscous damper. The equations of motion for the coupled system shown in Fig. 1 are written as

$$(\hat{M}_{cyl}+\hat{M}_{rnes})\frac{\mathrm{d}^2y_1}{\mathrm{d}t^2}+\hat{K}_{cyl}y_1 = F_L+\hat{M}_{rnes}r_0\frac{\mathrm{d}}{\mathrm{d}t}\left(\frac{\mathrm{d}\theta}{\mathrm{d}t}\sin\theta\right) \tag{1a}$$

$$\hat{M}_{rnes}r_0^2\frac{\mathrm{d}^2\theta}{\mathrm{d}t^2}+\hat{C}_{rnes}\frac{\mathrm{d}\theta}{\mathrm{d}t} = \hat{M}_{rnes}r_0\frac{\mathrm{d}^2y_1}{\mathrm{d}t^2}\sin\theta \tag{1b}$$

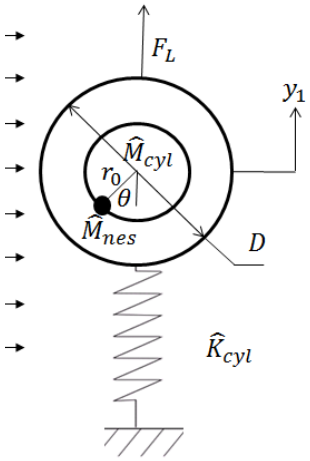

Figure 1: Schematic of a cylinder in flow with a rotational NES.

where $\hat{M}_{cyl}$ and $\hat{K}_{cyl}$ are the mass and the stiffness per unit length of cylinder, respectively. The NES mass and damping per unit length of the cylinder are denoted by $\hat{M}_{rnes}$ and $\hat{C}_{nes}$, respectively. Nondimensionalizing the time and the length by scaling with U_0/D and D, respectively, dimensionless variables are introduced as $Y_1 = y_1/D$, $\bar{r}_0 = r_0/D$, and $\tau = tU_0/D$. The term involving the lift force F_L is nondimensionalized using the dimensionless density $m^* = \rho_b/\rho_f$ and dimensionless lift coefficient $C_L = 2F_L/\rho_f U_0^2 D$ giving

$$\ddot{Y}_1+\omega_r^*Y_1 = \frac{2C_L}{\pi m^*}+\epsilon_r\bar{r}_0\frac{\mathrm{d}}{\mathrm{d}\tau}\left(\dot{\theta}\sin\theta\right) \tag{2a}$$

$$\ddot{\theta}+\lambda_r\dot{\theta} = \frac{\ddot{Y}_1}{\bar{r}_0}\sin\theta \tag{2b}$$

where we use the notation $\dot{(\,)} = \mathrm{d}(\,)/\mathrm{d}\tau$ and $\ddot{(\,)} = \mathrm{d}^2(\,)/\mathrm{d}\tau^2$. The dimensionless natural frequency of the cylinder supported on the linear spring is $\omega_r^* = \left(D^2/U_0^2\right)\left(\hat{K}_{cyl}/\left(\hat{M}_{cyl}+\hat{M}_{rnes}\right)\right)$. The dimensionless parameters characterizing the NES are the mass ratio $\epsilon_r = \hat{M}_{rnes}/(\hat{M}_{cyl}+\hat{M}_{rnes})$, radius ratio $\bar{r}_0$, and damping ratio $\lambda_r = D\hat{C}_{rnes}/(\hat{M}_{rnes}r_0^2U_0)$. In deriving the equations of motion, θ is taken to be positive counterclockwise, and $\theta = 0$ and $\theta = \pi$ correspond to fixed points of the system. In all the simulation results discussed in this paper, the initial conditions for the θ DOF are taken as $\theta(0) = \pi/2$ and $\dot{\theta}(0) = 0$. The lift coefficient C_L that drives the coupled system (2) is computed by solving the viscous incompressible Navier-Stokes equations via a multiscale/stabilized residue based finite-element approach developed in [3], the detailed description of computational model and validation results are discussed in [4] and references cited therein. The structural dynamical equations and the Navier-Stokes equations are solved in a staggered fashion as described by [4] to obtain the fully couple solution at each time-step. The flow Reynolds number is defined based on the cylinder diameter (D), the uniform upstream velocity (U_0), and kinematic viscosity ν as $Re = U_0D/\nu$.

Critical Re for the motionless cylinder

We first confirm that for a motionless cylinder, the Hopf bifurcation occurs at $Re_c \approx 47$ in our computational model. Any small disturbance in the flow past a cylinder with $Re > Re_c$ will grow in time, leading to temporal instability of the steady symmetric flow resulting in a limit-cycle oscillation of the lift force on the cylinder. As the flow Reynolds

number approaches Re_c, the temporal growth rate becomes extremely small and requires a very long-time integration if we rely solely on the numerical round-off error as the source of asymmetry to trigger the instability. In order to expedite the process, we introduce a small temporal disturbance in the upstream inlet boundary condition to perturb the steady-symmetric solution. Based on this approach, we determine the narrow range of Re_c for the motionless cylinder as $46.7 \leq Re_c \leq 46.8$, which agrees with the results available in the literature [1].

VIV of sprung cylinder at subcritical Re

In this section, we discuss the subcritical Re VIV of a elastically supported cylinder with mass ratio $m^* = \rho_b/\rho_f = 10$ and dimensionless frequency $F_n^* = \left(2\pi\nu/D^2\right)\sqrt{\left(\hat{K}_{cyl}/\hat{M}_{cyl}\right)}$. By perturbing the inlet velocity boundary condition, we identify a narrow range of Re that bounds Re_c. We perform this computational study for two different values of stiffness of the cylinder support, and show that the range of Re for synchronized (State of the coupled system in which the frequency of the lift force deviates from its natural shedding frequency and coincides with the natural frequency of the cylinder, resulting in large amplitude vibration.) VIV depends on the stiffness of the support. We illustrate this

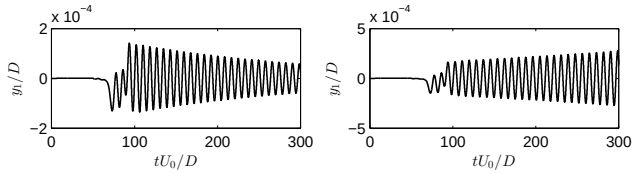

(a) $Re = 21$ (b) $Re = 22$

Figure 2: Time series with decaying and growing solutions at the beginning of the synchronization Re_c for $1/F_n^* = 0.35$ of the cylinder without NES.

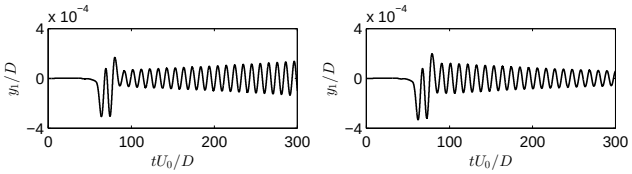

(a) $Re = 29$ (b) $Re = 30$

Figure 3: Time series with growing and decaying solutions at the end of the synchronization Re_c for $1/F_n^* = 0.35$ of the cylinder without NES.

synchronization for a particular stiffness value inferred by $1/F_n^* = 0.35$. On the lower end, synchronization begins in the narrow range of $21 \leq Re \leq 22$; the corresponding time series are shown in Fig. 2. For the same natural frequency of the cylinder, we observe that the upper end of synchronization is located in the narrow range $29 \leq Re \leq 30$ as shown in Fig. 3. Thus, the synchronization regime for this stiffness spans the range $22 \leq Re \leq 29$. A similar analysis performed for $1/F_n^* = 0.3$, we find the range of synchronization to be $24 \leq Re \leq 34$. Thus, we see that the range of Re over which synchronization is possible depends on the natural frequency of the cylinder.

Effect of a rotational NES on Re_c of sprung cylinder

In this section, we discuss the effect of introducing an essentially nonlinear rotating NES into the cylinder on the critical Re of the sprung cylinder. The NES parameters are fixed at $\bar{r}_0 = 0.3$, $\epsilon_r = 0.3$, and $2.7739 \leq \lambda_r \leq 3.7726$. These NES parameter are not optimized for any specific objective; our intention is to study the general effect that targeted energy transfer due to NES on the synchronization regime at a particular stiffness. For a cylinder stiffness inferred by $1/F_n^* = 0.35$, we identify a narrow range of Re that defines onset and end of synchronization. On the lower end, the synchronization begins in the narrow range of $25 \leq Re \leq 26$, and we observe that the upper end of synchronization is located in the narrow range $33 \leq Re \leq 34$. Thus, the synchronization regime for this stiffness spans the range $26 \leq Re \leq 33$. Hence, the presence of rotational NES delays the instability and shifts the synchronization regime to higher Re range compared to the system without the NES at the same stiffness.

Conclusions

For a sprung cylinder, VIV is possible below the Hopf bifurcation Re_c of the stationary cylinder. The critical Re above which VIV is possible depends on the natural frequency of the cylinder. In the subcritical Re (below the Hopf bifurcation Re_c) flow, synchronization occurs over a range of Re, with the synchronization range dependent on the natural frequency of the cylinder. The effect of the rotational NES on the bifurcation Re is to delay the onset of synchronization.

References

[1] Cossu, C. and Morino, L. (2000) On the Instability of a Spring-Mounted Circular Cylinder in a Viscous Flow at Low Reynolds Numbers. *Journal of Fluids and Structures* **14**:183-196.

[2] Gendelman, O. V. and Sigalov, G. and Manevitch, L. I. and Mane, M. and Vakakis, A. F. and Bergman, L. A. (2012) Dynamics of an Eccentric Rotational Nonlinear Energy Sink. *Journal of Applied Mechanics* **79**:011012-9.

[3] Masud A. and Calderer R. (2009) A variational multiscale stabilized formulation for the incompressible Navier-Stokes equations. *Computational Mechanics* **44**:145-190.

[4] Tumkur, R. K. R. and Calderer, R. and Bergman, L. A. and Vakakis, A. F. and Masud, A. and Pearlstein, A. J. (2012) Computational Study of Vortex-Induced Vibration of a Sprung Rigid Circular Cylinder with a Strongly Nonlinear Internal Attachment. *Journal of Fluids and Structures* **51**:214-232.